

The 10 Å phase at high pressure by first principles calculations and implications for the petrology of subduction zones

Patrizia Fumagalli ^{a,*}, Lars Stixrude ^b

^a *Dipartimento di Scienze della Terra, Università degli Studi di Milano, Milano, Italy*

^b *Department of Geological Sciences, University of Michigan, Ann Arbor, Michigan, United States*

Received 1 February 2007; received in revised form 2 May 2007; accepted 19 May 2007

Available online 26 May 2007

Editor: G.D. Price

Abstract

The structure and the physical properties of the 10 Å phase, $\text{Mg}_3\text{Si}_4\text{O}_{10}(\text{OH})_2 \cdot n\text{H}_2\text{O}$, with $n=0$, $n=1$ and $n=2$ is explored over a wide range of pressure with density functional theory in the local density (LDA) and generalized gradient approximations (GGA). The static equation of state depends strongly on the amount of water ($n=0$: $V_0=218.1(4) \text{ \AA}^3$, $K_0=37.0(6) \text{ GPa}$, $K'_0=14.0(2)$; $n=1$: $V_0=226.6(3) \text{ \AA}^3$, $K_0=54.2(5) \text{ GPa}$, $K'_0=17.2(2)$, $n=2$: $V_0=238.9(4) \text{ \AA}^3$, $K_0=38.2(12) \text{ GPa}$, $K'_0=24.0(6)$). All the investigated structures present a layer offset with respect to the ideal phlogopite like stacking along the x direction that influences the beta angle: tetrahedral rings and water molecules are not exactly aligned along the c nor the c^* directions in the $n=1$ and $n=2$ structures. Water is bound to the tetrahedral sheets and is located off the mid-plane of the interlayer. The water dipole vector lies almost parallel to the tetrahedral sheets at zero pressure; the angle it forms with the ab plane increases with pressure in both $n=1$ (up to 80°) and $n=2$ (up to 50°) structures. Water molecules act both as acceptor and donor oxygen groups for hydrogen bonds. Water oxygens accept hydrogen from the intra-layer hydroxyls, leading to H-bonds at the boundary between the weak and the strong limit, in agreement with the relatively high Raman frequency at 3620 cm^{-1} assigned to this vibrational mode. Water molecules donate hydrogen to basal oxygens of the tetrahedral sheet. Interactions between water molecules and basal oxygens are complicated by the occurrence of polifurcated, mainly asymmetric, bent hydrogen bonds. Nonetheless, within the stability field of the 10 Å phase, LDA results yield distances between basal oxygens and water hydrogen that fall between the weak and strong limit in agreement with Raman signals at 3672 and 3593 cm^{-1} . GGA simulations suggest even stronger interactions between water molecules and basal oxygens.

© 2007 Elsevier B.V. All rights reserved.

Keywords: first principles calculations; 10 Å phase; hydrous phase; high pressure; subduction

1. Introduction

Hydrous phases strongly influence chemical and physical processes at subduction zones, and have been proposed as carriers of water to the deep mantle and as

storage sites of water (Frost, 1999). The 10 Å phase, $\text{Mg}_3\text{Si}_4\text{O}_{10}(\text{OH})_2 \cdot n\text{H}_2\text{O}$, was first synthesised in the $\text{MgO-SiO}_2\text{-H}_2\text{O}$ (MSH) system (Sclar et al., 1965). It is widely accepted that it consists of a 2:1 phyllosilicate structure with interlayer water (Fumagalli et al., 2001; Pawley et al., 2004; Comodi et al., 2005). The speciation of hydrogen within the structure is therefore unusual as both hydroxyls and water molecules occur, a feature that

* Corresponding author.

E-mail address: patrizia.fumagalli@unimi.it (P. Fumagalli).

is shared by only one other high pressure mineral, lawsonite (Libowitzky and Rossman, 1996). The hydrogen content in the 10 Å phase appears to vary with run duration (Fumagalli et al., 2001), explaining the wide range of H₂O suggested by previous investigations ($n=0.65-2$, H₂O=7.6–13.1 wt.%, Wunder and Schreyer, 1992 and reference therein). As compared with other dense hydrous magnesium silicates (DHMS) (Angel et al., 2001) such as phase A (H₂O=11.8 wt.%), super-hydrous B (H₂O= 5.8 wt.%), phase D (H₂O=18 wt.%) and phase E (H₂O=11–18 wt.%), the 10 Å phase is among those with the highest water content and therefore a good candidate for storing and transporting H₂O at high pressure.

The 10 Å phase, slightly deviating from the simple MSH composition in incorporating Al, has been found to develop at the expense of chlorite at pressure above 4.8 GPa, 680 °C in lherzolitic compositions (Fumagalli and Poli, 2005). Phase relations together with its ability to incorporate a variable amount of water indicate that, in aluminum-bearing compositions, it might play an important role in triggering intermediate depth earthquakes along double seismic zones at H₂O under-saturation (Fumagalli and Poli, 2005). Natural evidence of the 10 Å phase as inclusions in olivine (100 nm in size) have been recently suggested by FTIR and TEM investigations (Kishina et al., 2001). Textures suggest that the 10 Å phase formed at high pressure and that it has been partially or totally replaced by talc + serpentine during exhumation.

Due to the petrological implications for the global water cycle related to the occurrence of the 10 Å phase at high pressure, its structural and thermodynamic parameters have been investigated both theoretically (Bridgeman et al., 1996; Bridgeman and Skipper, 1997; Wang et al., 2004, 2005) and experimentally (Pawley et al., 1995; Chinnery et al., 1999; Fumagalli et al., 2001; Pawley et al., 2004; Comodi et al., 2005, 2006). Although all structural models feature water molecules sandwiched between TOT layers, the detailed atomic positions remain uncertain, as does the existence, the nature, and the strength of hydrogen bonds. In particular, the nature of the interactions between interlayer water and the TOT layers is unclear and a variety of hydrogen bonding geometries have been proposed.

Raman spectroscopy and X-ray powder diffractometry define a model structure combining a mica-like stacking (monoclinic space group), and talc-like TOT sheets with interlayer water molecules (Fumagalli et al., 2001). A phlogopite type stacking has been further confirmed by both neutron powder diffraction on deuterated samples of the 10 Å phase (Pawley et al., 2004) and by a recent structure refinement based on

single crystal X ray diffraction (Comodi et al., 2005). Regarding the location of interlayer water, Comodi et al. (2005) proposed two alternative models that are equally consistent with their observations, one in which the water oxygens are located at the interlayer mid-plane, and another in which they are displaced by 0.27 Å from the mid-plane. Hydrogen positions have not yet been determined by diffraction methods.

From a theoretical point of view the type of stacking and the detailed location of water molecules within the interlayer is still uncertain. Previous theoretical studies have been based on semi-empirical force fields (Wang et al., 2004) and density functional theory computations without full structural relaxation (Bridgeman et al., 1996). Both talc and phlogopite type stacking were found to be energetically stable and water has been located both at the mid-plane (Bridgeman et al., 1996) and off the mid-plane, arranged in two sublayers associated with the two tetrahedral sheets (Wang et al., 2004). In order to unravel and explore the energetics of the 10 Å phase as a function of water content, and to determine the most favorable structure at high pressure, we have carried out a first principles study. Ours is the first density functional theory based study of the 10 Å phase to include full structural relaxation and careful convergence tests, technical issues that we find to be essential for yielding accurate results. First principles methods have proved to be a powerful tool to investigate high pressure structures and thermodynamic properties, including those of hydrous phases (Stixrude, 2002; Mookherjee and Stixrude, 2006). Results, including the predicted equation of state, lattice parameters, internal structural parameters and H configurations as a function of pressure will be useful for understanding the stability of this phase, the nature of hydrogen bonding at high pressure, and for designing new experiments.

1.1. Computational methods: the model structure of the 10 Å phase

Calculations are based on density functional theory and have been performed using the Vienna Ab Initio Simulation Package (VASP, Kresse and Hafner, 1993; Kresse and Furthmüller, 1996a,b). Two widely used approximations have been made to describe the exchange-correlation functional: 1) the local density approximation (LDA) and 2) the generalized gradient approximation (GGA). In all cases, we use ultra-soft Vanderbilt pseudopotentials (Vanderbilt, 1990; Kresse and Hafner, 1994).

We perform complete relaxations of the structure, including cell parameters and all internal coordinates at

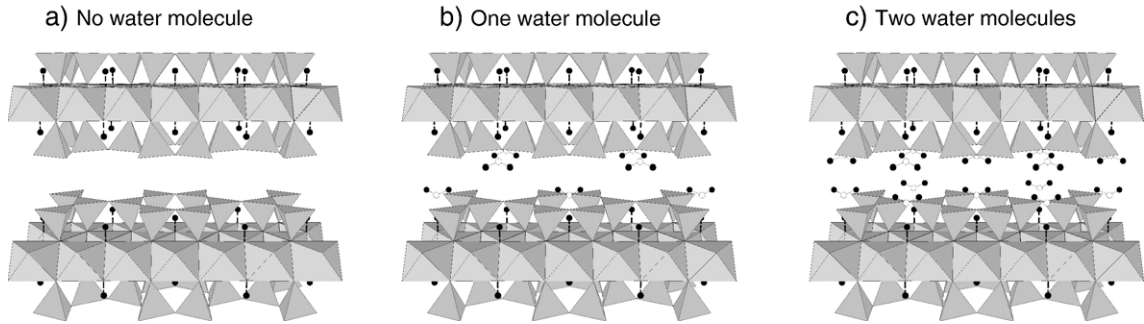


Fig. 1. (100) projections of the starting model structures of the 10 Å phase at different water content.

constant volume and static (0 K) conditions. We analyse compressional and tensional behavior. Tests showed that a Monkhorst–Pack (1976) $2 \times 2 \times 2$ k-point mesh and a cut off energy of 600 eV were sufficient to converge the total energy to within 0.1 meV and the pressure to within 0.03 GPa.

The initial estimates of structures, which are used to initiate full relaxations, are based on the model proposed by Fumagalli et al. (2001) who derive a model structure based on a combination of Raman spectroscopy and X-ray powder diffractometry on samples synthesised at high pressure. A water content of 2 molecules per formula unit has been considered as the maximum amount that can be incorporated into the structure. Water molecules are located off the mid-plane in order to take into account their strong interaction with the TOT sheet as indicated by Raman spectroscopy (Fumagalli et al., 2001). During structural relaxation the position of water molecules, as well as all other atoms and cell parameters are free to move following energy minimization. In order to unravel the stability and the nature of H-bonds within the structure at different water content three different structures have been considered as starting models (Fig. 1): 1) the two water molecules structure of Fumagalli et al. (2001) using a primitive C2/m unit cell; 2) a zero water structure derived from the 2 water structure by removing all water molecules, i.e. the primitive C2/m unit cell is maintained; 3) a 1 water molecule structure, where half of the water molecules have been removed in such a way as to preserve the inversion center and resulting in a $\sqrt{2} \times \sqrt{2} \times 1$ primitive unit cell, identical to the conventional unit cell of the two-water and zero-water structures. In order to limit the number of atoms and minimize the computational cost, primitive cells rather than conventional cells were used in all calculations (i.e. 21 atoms for the no water structure, 48 for the 1 water structure, 27 atoms for the 2 water structure). Nonetheless lattice parameters are

expressed in terms of the conventional c -centered cell for all cases to facilitate comparison.

2. Results

2.1. Layer stacking

All three structures show significant layer offset, unlike phlogopite, in which TOT sheets are aligned along the c^* direction and $\beta = 100^\circ$ (Fig. 2). In the 10 Å phase, we find that the β angle decreases systematically with increasing water content. The $n=0$ structure shows $\beta = 108^\circ$ at the experimental zero pressure volume,

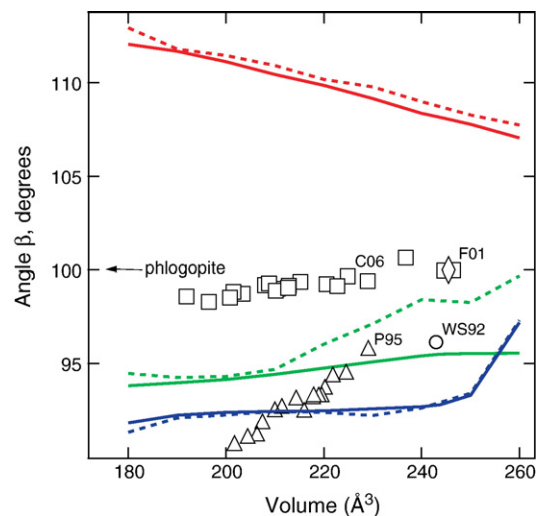


Fig. 2. Beta angle vs. volume. In red the no water structure, in green the 1 water molecule structure, in blue the 2 water molecules structure. Straight lines are LDA results, dashed lines are GGA results. Open squares: in situ experimental data (Comodi et al., 2006 — C06); open triangles: in situ experimental data (Pawley et al., 1995 — P95); open circle: experimental datum from Wunder and Schreyer (1992) — WS92; open diamond: experimental datum from Fumagalli et al. (2001) — F01. (For interpretation of the references to color in this figure legend, the reader is referred to the web version of this article.)

Table 1
Equation of state parameters of the 10 Å phase

Data	V_0 (Å ³)	K_0 (GPa)	K'_0	$K_0K''_0$	Reference
0 W	218.1(4)	37.0(6)	14.0(2)	−169(7)	This work
1 W	226.6(3)	54.2(5)	17.2(2)	−260(7)	This work
2 W	238.9(4)	38.2(12)	24.0(6)	−505(28)	This work
0 W 300 K	222.3	28	17		This work
1 W 300 K	229.4	42	21		This work
2 W 300 K	245.6	15	55		This work
10 Å phase Exp	229.95	32.2(55)	9.2(28)	–	Pawley et al. (1995)
10 Å phase Exp	246.45(15)	39(3)	12.5(8)	–	Comodi et al. (2006)
Talc Theory	217.5(1)	37.8(4)	13.6(2)	–	Stixrude (2002)
Talc 300K	221.8(2)	29(5)	17	−250	Stixrude (2002)
Talc Exp	226.9(1)	41.6(9)	6.5(4)	–	(*)
Phl Exp	248.55(5)	54(2)	7(1)	–	Comodi et al. (2004)
Phl Exp	244.32	49.7(5)	8.59(19)	–	Pavese et al. (2003)

Numbers in parentheses represent uncertainties in the last digit. Theoretical values marked “300 K” indicate those corrected for zero point motion and 300 K thermal pressure using thermal properties identical to those assumed for talc (Stixrude, 2002). 10 Å: 10 Å phase, Phl: phlogopite, Exp: Experimental data. (*) V_0 from Perdikatsis and Burzlaff (1981); K_0 and K'_0 from Pawley et al. (1995).

corresponding to a layer offset $\Delta=1.53$ Å. This layer offset is readily understood on energetic grounds as it is nearly identical to the value that minimizes O–O repulsion across the inter-layer.

The water-bearing structures both have values of β smaller than phlogopite, reflecting the interaction of water molecules with each other, and with the TOT sheets. For the $n=1$ structure, the value of β is only slightly smaller than phlogopite at the experimental zero-pressure volume within GGA and substantially smaller in the case of LDA. In the case of LDA, $\beta=96^\circ$, and $\Delta=0.73$ Å. GGA and LDA converge on compres-

sion, both showing the β angle decreasing on compression, and predict $\beta=95\text{--}96^\circ$ within the stability field of the 10 Å phase (4.0–7.0 GPa, 216–210 Å³). The $n=2$ structure exhibits a significantly smaller value of β than the $n=1$ structure over the entire range studied, except at $V=260$ Å³, which is under tension (negative pressure). At volumes smaller than $V=260$ Å³, the monoclinic angle decreases slightly with compression in the $n=2$ structure. At the experimental zero pressure volume, both LDA and GGA show $\beta=93^\circ$ and $\Delta=1.26$ Å.

The predicted values of the β angle for the $n=1$ and $n=2$ structures are consistent with a range of experimental values that have been obtained at zero pressure: $95\text{--}100^\circ$ (Wunder and Schreyer, 1992; Pawley et al., 1995; Fumagalli et al., 2001; Comodi et al., 2006). Within the stability field of the 10 Å phase, our results fall in between high pressure experimental results of Pawley et al. (1995) and Comodi et al. (2006).

2.2. Volume, equation of state and compression

With the addition of water, the volume of the 10 Å phase increases systematically, with increase in the c^* direction accounting for most of the variation (Tables 1 and 2, Fig. 3). We may analyze these changes in terms of the partial molar volume of water

$$\langle \bar{V}_w \rangle = [V(n) - V(0)]/n$$

where V is the volume per formula unit (per two hydroxyls, i.e. per $\text{Mg}_3\text{Si}_4\text{O}_{10}(\text{OH})_2$ in the case of $n=0$) and n is the number of water molecules per formula unit. The quantity on the left hand side of the equation is formally the mean value of the partial molar volume of water over the compositional range $0\text{--}n$ (Sposito and Prost, 1982). From our results, the difference in volume between the $n=1$ and $n=0$ structures per water molecule is 2.6 cm³/mol, and between the $n=2$ and $n=0$ structures is 3.1 cm³/mol. These values may be compared with the molar volume of water or ice 1 h ($V_w^0=18$ cm³/mol). The much smaller apparent volume of water in the 10 Å phase

Table 2
Lattice parameters and linear moduli in GPa at ambient pressure and static conditions

Data	a_0	b_0	c_0^*	c_0^*/a_0	V_0	K_a	K_b	K_c	K_V
0 W	5.270	9.086	9.091	1.72	218.1	408(12)	244(7)	53.2(12)	39.5
1 W	5.273	9.137	9.397	1.78	226.6	663(11)	416(8)	74.5(80)	57.7
2 W	5.282	9.182	9.839	1.86	238.9	602(8)	443(7)	41.6(15)	35.8
Exp	5.323	9.203	10.061	1.89	246.4	833(11)	581(30)	41.7(3)(**)	37.2

Experimental data (Exp) are from Comodi et al. (2006); $c_0^*=c\sin\beta$ refers to the projection of c lattice parameter to c^* direction. (**) K_c at zero pressure calculated according to the relation $c/c_0=0.876(2)+0.116 e^{-P/6.7(5)}$ of Comodi et al. (2006). K_V derived from linear moduli.

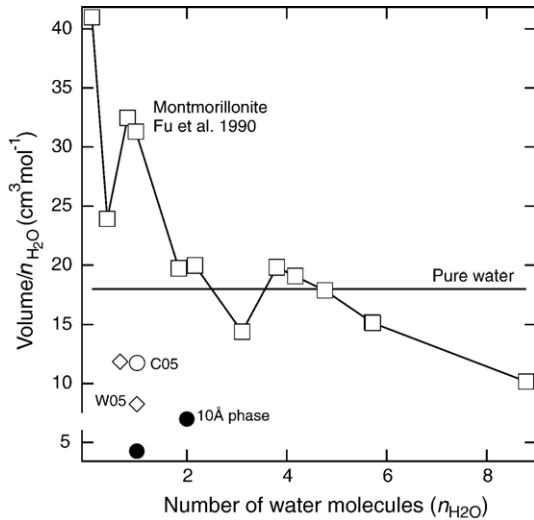


Fig. 3. Volume per water molecule vs. number of water molecules for the 10 Å phase. Black circles: LDA 300K values; open diamonds: theoretical predictions by Wang et al. (2005) (W05) at 0.1 MPa, 300 K, the volume at $n=0$ was assumed from their results on talc structure; open circles: experimental results from Comodi et al. (2005) (C05) for which $n=1$ has been assumed and the experimental volume of talc has been considered as V at $n=0$. Open squares: experimental results for Na-montmorillonite (Na-Mt) from Fu et al. (1990); the experimental volume for Na-Mt (VNa-Mt) was computed from the reported $d(001)$ spacings and the assumption that the area of the $a-b$ plane is identical to that of Ca-Mt refined by Viani et al. (2002), VNa-Mt at $n=0$ has been taken from Cygan et al. (2004).

structure reflects the strong interaction between water molecules and the TOT sheets, and the different arrangement of water molecules in the phyllosilicate as

compared with that in pure water or ice. The strong interaction between water molecules and TOT sheets in the 10 Å phase is further emphasized by comparison with water-bearing clays, such as Na-montmorillonite. In this material, $\langle \bar{V}_w \rangle$ is larger than V_w^0 , reflecting much weaker interactions between water and silicate components.

The equation of state calculated within the local density approximation and general gradient approximation under static conditions are represented in Fig. 4 and Table 1. The LDA equation of state of the $n=0$ structure is essentially identical to that of talc (Stixrude, 2002). Differences in stacking between these two structures appear to have a negligible influence on the equation of state within LDA. GGA results are somewhat more sensitive to the differences between talc and our $n=0$ structure.

The $n=1$ and $n=2$ structures are substantially stiffer than the water-free structure. This is reflected in the steeper pressure–volume slopes of the equation of state (Fig. 4), the larger bulk modulus of the $n=1$ as compared with the $n=0$ structure, and the larger value of K'_0 of the $n=2$ as compared with the $n=0$ structure. The greater stiffness upon addition of water reflects the interaction of water molecules within the interlayer, including H–H and O–O repulsions. Remarkably, the $n=2$ structure has a smaller value of K_0 than the $n=1$ structure, although the value of K'_0 of the $n=2$ structure is much greater than that of the $n=1$ structure, so that the $n=2$ structure rapidly becomes stiffer than the $n=1$ structure on compression. The relative values of K_0 of the water bearing structures reflect the larger volume of the $n=2$ structure (Anderson and Nafe, 1965).

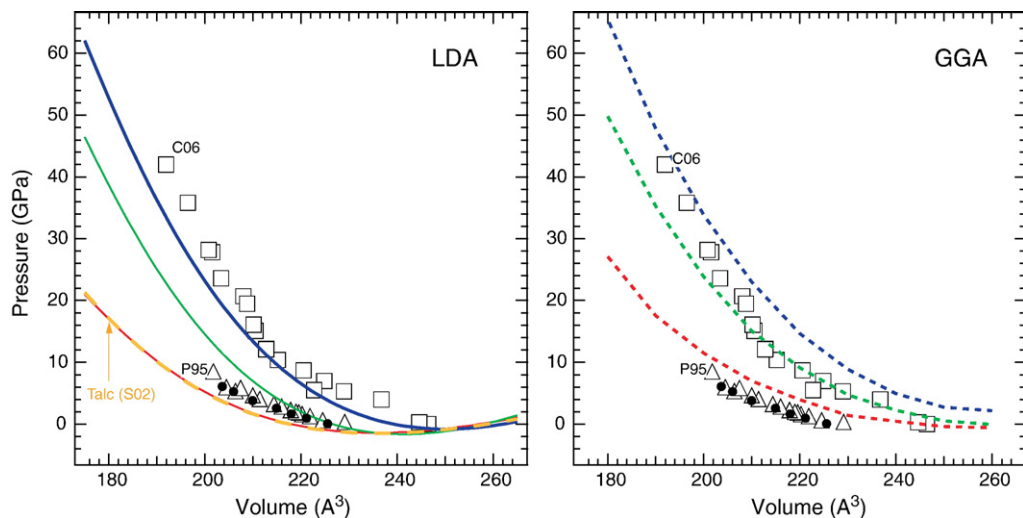


Fig. 4. LDA (left) and GGA (right) Equation of State for the three structures investigated: 0 water molecule structure (red); 1 water molecule structure (green); 2 water molecules structure (blue). Dashed yellow line is Equation of State of Talc from Stixrude (2002) — S02. Symbols are available experimental data (triangles: Pawley et al., 1995 — P95; open squares: Comodi et al., 2006 — C06). Small black circles are experimental data on talc by Pawley et al. (1995). (For interpretation of the references to color in this figure legend, the reader is referred to the web version of this article.)

Table 3
Properties of polyhedra at selected values of the unit cell volume

Volume (Å ³)	P_{static} (GPa)	V_{Mg} (Å ³)	V_{Si} (Å ³)	Q_{Mg}	Q_{Si}	ψ
<i>0 Water structure</i>						
250	-0.953	11.538	2.175	1.0092	1.0000	58.558
243.81	-1.054	11.533	2.175	1.0092	1.0000	58.565
240	-1.029	11.540	2.175	1.0091	1.0000	58.538
230	-1.436	11.566	2.180	1.0091	1.0000	58.539
220	-0.392	11.474	2.174	1.0090	1.0000	58.527
210	1.721	11.293	2.165	1.0081	1.0001	58.333
200	5.388	11.001	2.151	1.0072	1.0004	58.129
190	10.201	10.698	2.137	1.0059	1.0010	57.804
180	17.201	10.347	2.118	1.0046	1.0019	57.430
<i>1 Water structure</i>						
250	-1.286	11.613	2.185	1.0094	1.0003	58.598
243.81	-1.446	11.622	2.186	1.0094	1.0003	58.598
240	-1.598	11.639	2.187	1.0093	1.0003	58.578
230	-0.788	11.574	2.178	1.0093	1.0006	58.586
220	1.945	11.395	2.149	1.0094	1.0012	58.602
210	7.007	11.107	2.105	1.0096	1.0020	58.611
200	14.611	10.742	2.050	1.0101	1.0029	58.626
190	25.020	10.325	1.987	1.0112	1.0039	58.668
180	38.692	9.887	1.917	1.0129	1.0054	58.667
<i>2 Water structure</i>						
250	-0.645	11.639	2.203	1.0099	1.0009	59.704
243.81	-0.799	11.666	2.208	1.0098	1.0009	59.705
240	-0.188	11.624	2.205	1.0099	1.0010	59.704
220	6.437	11.231	2.162	1.0100	1.0014	59.715
210	13.536	10.862	2.114	1.0101	1.0021	59.738
200	23.235	10.439	2.057	1.0099	1.0033	59.782
190	36.137	9.966	1.992	1.0098	1.0050	59.845
180	52.774	9.471	1.920	1.0096	1.0077	59.937

The calculated static pressure is also shown for reference.

In order to compare our results with available experimental data we keep in mind some important considerations: i) by comparing to experimental results performed at room temperature, we need to take into account the contribution of lattice vibrations. As the thermal properties of the 10 Å phase are not well known, we have assumed that the contribution to the pressure from zero-point motion and 300 K thermal pressure are identical to those in talc as estimated by Stixrude (2002). ii) It is known that LDA systematically overbinds structures, leading to underestimation of the volume and overestimation of the bulk modulus (e.g. Stixrude, 2002) iii) Theoretical calculations correspond to the Reuss (uniform stress) lower bound on the bulk modulus whereas polycrystalline diffraction experiments measure a bulk modulus in between the Voigt and Reuss bounds that is therefore greater than the Reuss bound. The differences between the bounds can be large in particular for phyllosilicates, which tend to be highly

anisotropic (Stixrude, 2002); iv) In the case of diamond anvil cell experiments the typical X-ray scattering geometry tends systematically to underestimate compression (Duffy et al., 1995). This apparent stiffening of the equation of state arises from non-hydrostatic stress and is largest when no pressure medium is used, as in the experiments of Comodi et al. (2006).

In the light of such a general considerations, the experimental data of Pawley et al. (1995) are best explained by the $n=0$ structure. The zero pressure volume found in this experimental study is 3% larger than our estimate of the 300 K zero pressure volume of the $n=0$ structure. This difference is similar to that between the same level of theory and experiment in the case of talc (Stixrude, 2002). Furthermore, Pawley et al. (1995) found that their 10 Å phase results and talc showed the same compressibility behavior, a pattern that is incompatible with our results showing that the equation of state depends strongly on water content. Finally, we note that the experimental data of Pawley et al. (1995) on talc and the 10 Å phase overlap, suggesting that the 10 Å phase sample studied by Pawley et al. (1995) was in fact water free (Fig. 4).

Recent experimental data on a different sample (Fumagalli et al., 2001; Comodi et al., 2005, 2006) show a much larger zero pressure volume than the experiments of Pawley et al. (1995). Moreover, the high pressure data of Comodi et al. (2006) show an equation

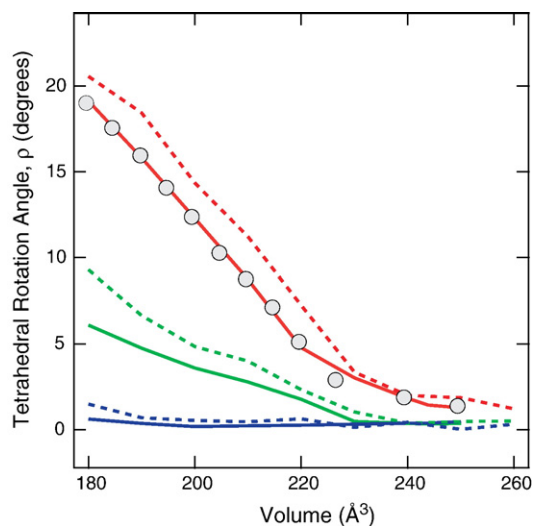


Fig. 5. Measure tetrahedral rotation angle vs. volume. In red the no water structure, in green the 1 water molecule structure, in blue the 2 water molecules structure. Straight lines are LDA results, dashed lines are GGA results. Grey circles are the theoretically predicted tetrahedral rotation angles for talc (Stixrude, 2002). (For interpretation of the references to color in this figure legend, the reader is referred to the web version of this article.)

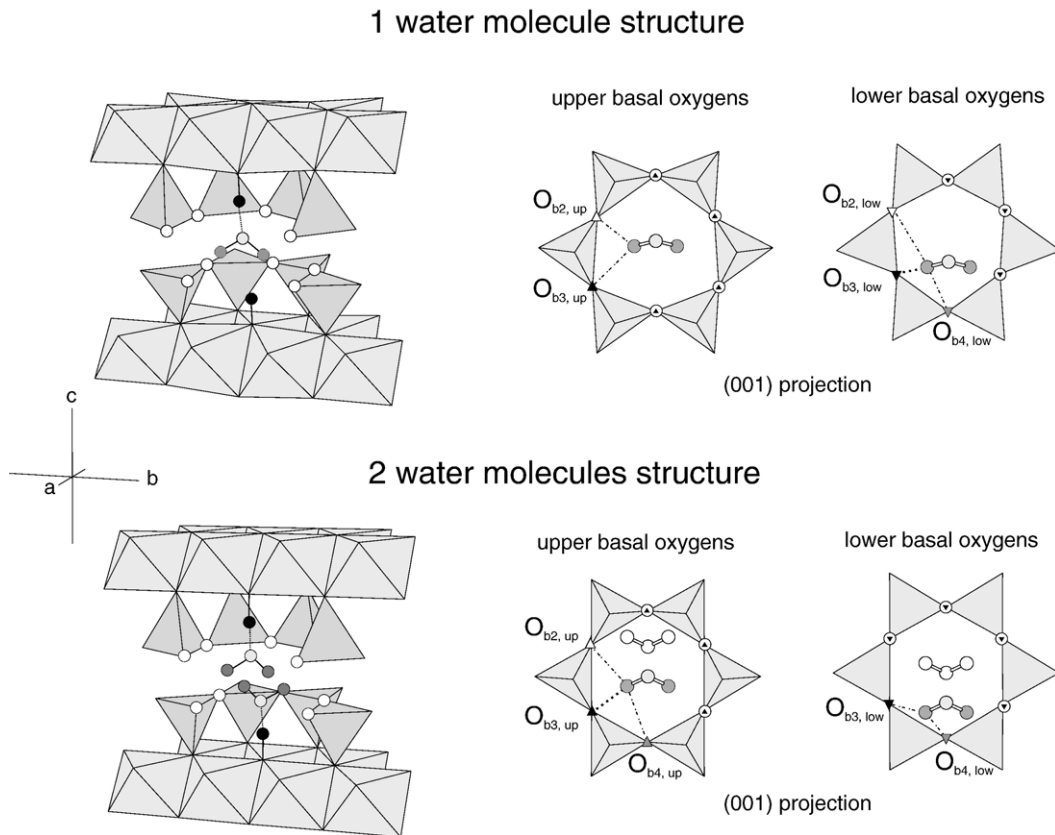


Fig. 6. High pressure hydrogen configuration in the 10 Å phase structures at different water content at the selected volume $V=180 \text{ \AA}^3$; light grey circles: water oxygens (O_w), black circles hydroxyls hydrogens (H_i), white circles are basal oxygens (O_b); hydrogen covalent bonds H_i-O_i and H_w-O_w : straight lines, $O_w \dots H_i-O_i$ and $O_w-H_w \dots O_b$ hydrogen bonds: dotted lines; (001) projections show the multi-furcated hydrogen bonds where the basal oxygen acting as major component are $O_{3, \text{low}}$ and $O_{3, \text{up}}$ for the $n=1$ and $n=2$ structures respectively; dotted-straight lines represent minor components (see also Figs. 8 and 9). Symbols in the (001) projections refer to plots in Fig. 8.

of state that is very different from talc. As the water content of the sample investigated by Comodi et al. (2006) has not been measured, our theoretical results might help in predicting the water content of the experimental sample.

Our results indicate that the $n=2$ structure best explains the experimental observations after accounting for phonon excitation as discussed above. The predicted 300 K volume of the $n=2$ structure is only 0.04% less than experiment. The remaining discrepancy is in agreement with the expected sign of the LDA error. The experimental value of K_0 (Comodi et al., 2006) is considerably greater than our predicted 300 K value for $n=2$. This discrepancy is also apparent in the trend of the equation of state (Fig. 4), which is considerably stiffer in the experimental data than in our theoretical results. This discrepancy might be explained by the influence of non-hydrostatic stress in the experimental set up due to the lack of the pressure medium, or to the

influence of grain–grain interactions on the value of the bulk modulus, causing it to deviate from the Reuss limit.

Cell parameters indicate that the compression of the 10 Å phase is highly anisotropic as expected (Table 2). All the structures have $K_a > K_b > K_c^*$, with the c^* -axis the most compressible. Compressional anisotropy increases with water content: for $n=0$, the c^* -axis is almost five times more compressible than the b -axis, while it is 10 times more compressible for $n=2$. The $n=2$ structure is approximately 80 % softer along c^* than the $n=1$ structure. The a – b plane is much stiffer in the water bearing structures than in the $n=0$ structure, by approximately 50%. The increased stiffness reflects the interactions among the water molecules including H–H and O–O repulsion, and between the water molecules and the TOT sheets. In all the structures we studied, the b -axis is more compressible than the a -axis, opposite their relative magnitudes in talc (Stixrude, 2002): the b -axis is approximately 1.7 times more

compressible than the a -axis for $n=0$, while it is 1.4 times more compressible for $n=2$.

As with our results, in situ experiments (Comodi et al., 2006) also find that the c^* direction is much more compressible than the a - b plane, and that the a direction is stiffest. The experimental values for a , and b linear compressibilities are substantially greater than our theoretical results. This pattern reflects the larger value of the bulk modulus in the experiments as compared with our results, as discussed above.

The very different patterns of compression in the $n=0$ structure and talc on the one hand, and the water-bearing structures on the other can be understood by examining the variation of polyhedral geometries with compression (Table 3a, b, c). For example, the quadratic elongation Q (Robinson et al., 1971) behaves differently in water-free vs. water-bearing structures. In the $n=0$ structure tetrahedra become more distorted and octahedral become more regular as pressure increases, similar to the behavior found in talc at high pressure (Stixrude, 2002). In contrast the $n=1$ and $n=2$ structures show that both tetrahedra and octahedra become more distorted as pressure increases although the distortion is of smaller magnitude than in the $n=0$ structure.

The effect of pressure on polyhedra distortion is related to the octahedral tilt angle, ψ defined as the angle between the octahedral body-diagonal and the c^* direction (Bailey, 1998) and the tetrahedral rotation angle, α defined as half the mean value of the angle formed by three oxygens of the inner surface ring less 120° . In comparison with the ideal value of $\cos^{-1}(1/3^{-1/2}) = 54.73^\circ$, the larger value of ψ obtained in all the three structures shows a flattening of the octahedral sheets. The decrease of ψ on compression in the $n=0$ structure indicates a relative thickening of the octahedral sheet, as also found in talc (Stixrude, 2002). In contrast in the water-bearing structures the ψ angle slightly increases with pressure indicating a further flattening of the octahedral sheets. Furthermore the extent of additional compression-induced flattening increases with increasing water content: $\Delta\psi = \psi_{250} - \psi_{180} = 0.07$ for $n=1$; and $\Delta\psi = 0.23$ for $n=2$. The tetrahedral rotation angle (Fig. 5) shows that the water free structure undergoes the greatest distortion of the tetrahedral sheet on compression. In the $n=0$ structure, α increases on compression to 20° over the range of volume studied here, nearly identical to previous results for talc (Stixrude, 2002), whereas, α differs from ideal by only a few degrees in the $n=2$ structure and by less than 6° in the $n=1$ structure. The lesser tetrahedral rotation in the case of the water bearing structures is in agreement with the greater stiffness of the a - b plane in these structures. It appears

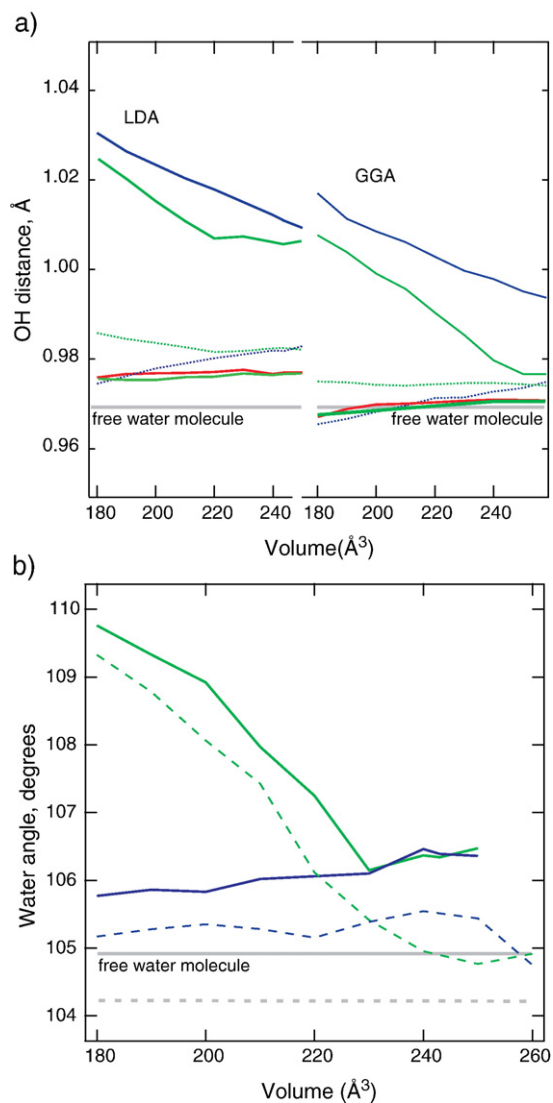


Fig. 7. Hydrogen covalent bonds in a) hydroxyls (straight lines: LDA; dashed lines: GGA) and water molecules (dotted lines) and b) water molecule angles vs. volume. Red: no water structure; green: 1 water structure; blue: 2 water structure. Distances and angles are compared with the geometry of the free water molecule (grey lines, straight: LDA, dashed: GGA) computed within the same theoretical framework (Xu and Goddard, 2004). (For interpretation of the references to color in this figure legend, the reader is referred to the web version of this article.)

that interaction with the water molecules forces the hexagonal rings of the T sheet to remain relatively open, instead of collapsing on compression as they do in water-free structures. The tetrahedral rotation angle has not been measured experimentally. Comodi et al. (2006) suggest the empirical expression $\cos\alpha = b/b_0$, where b_0 is the ideal value of the cell parameter b for which no tetrahedral

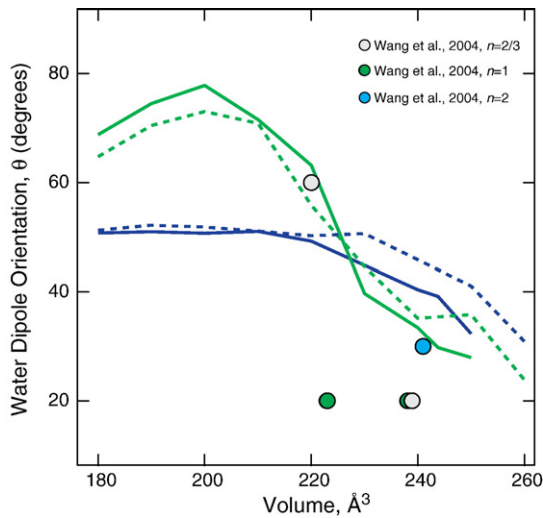


Fig. 8. Water dipole orientation with respect to the (001) plane vs. volume. In green the 1 water molecule structure, in blue the 2 water molecules structure. Straight lines are LDA results and dashed are GGA results. For $q=0^\circ$ water dipole is aligned parallel to the TOT sheet, for $q=90^\circ$ water dipole lies perpendicular with respect to TOT plane.

rotation is expected. This relationship was shown to capture the variation of the rotation angle in talc over a wide compression range (Stixrude, 2002), but its application to the 10 Å phase is suspect because the 10 Å phase compresses in a very different way than talc as indicated by the relative magnitudes of K_a , K_b , and K_c^* . Therefore, we believe that the very large values of α computed by Comodi et al. (2006) from the semi-empirical relationship (11° at $V=210.55 \text{ \AA}^3$, similar to our $n=0$ values) are probably unrealistic.

2.3. Hydrogen bonds

We find two types of hydrogen bonds in our water-bearing 10 Å phase structures (Fig. 6). The first involves the water oxygen, O_w , and the hydrogen H_i , and oxygen O_i of the inner hydroxyl, while the second involves the water oxygen, O_w , the water hydrogen, H_w , and the basal oxygen O_b :



Where the dash (–) indicates the hydroxyl and the ellipsis (...) indicates the weaker portion of the bond. There are several varieties of hydrogen bond of the second type involving several different basal oxygens. In the first type of hydrogen bond, water molecules act as the acceptor group whereas in the second type, water molecules act as donor group.

The presence of the first type of hydrogen bond is illustrated by the behavior of the inner hydroxyl (Fig. 7a). Whereas in the $n=0$ structure, the $H_i - O_i$ distance is essentially independent of compression, in the water bearing structures, this distance is longer and increases with compression. The $H_i - O_i$ distance increases from 1.0064 Å at $V=250 \text{ \AA}^3$ to 1.0247 at $V=180 \text{ \AA}^3$ in the $n=1$ structure for those hydroxyls associated with an interlayer water, and from 1.0093 Å at $V=250 \text{ \AA}^3$ to 1.0305 Å at $V=180 \text{ \AA}^3$ in the $n=2$ structure. This is the behavior expected of a hydrogen bond. The presence of hydrogen bonding is further illustrated by the $n=1$ structure. In this structure, half of the inner hydroxyls are associated with interlayer water, and the other half are not. Those hydroxyls that are not

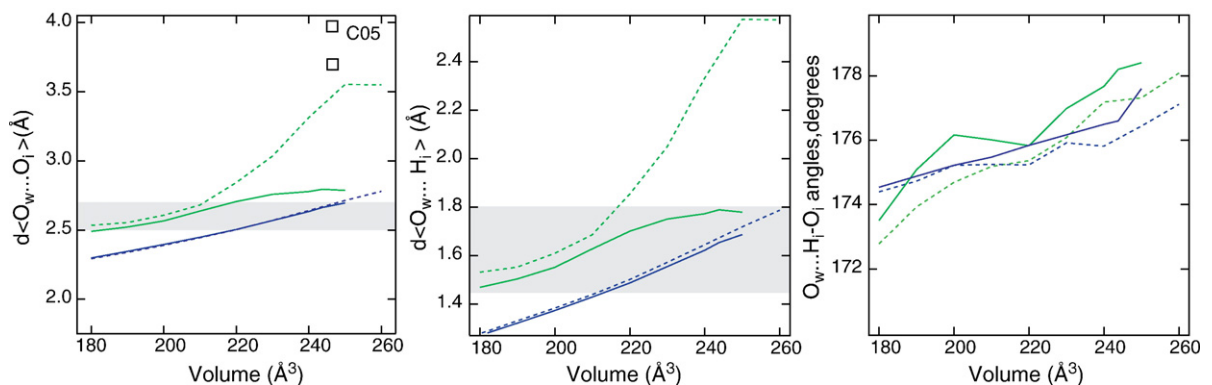


Fig. 9. $d\langle O_w \dots O_i \rangle$, $d\langle O_w \dots H_i \rangle$ distances and $O_w \dots H_i - O_i$ angles vs. volume, green: 1 water molecule structure; blue: 2 water molecules structure, open square: experimental by Comodi et al. (2005). The shaded area represent strong bonds region on the basis of $O \dots O$ and $O \dots H$ distances. Longer distances are weak H-bonds, shorter distances describe very strong bonds. (For interpretation of the references to color in this figure legend, the reader is referred to the web version of this article.)

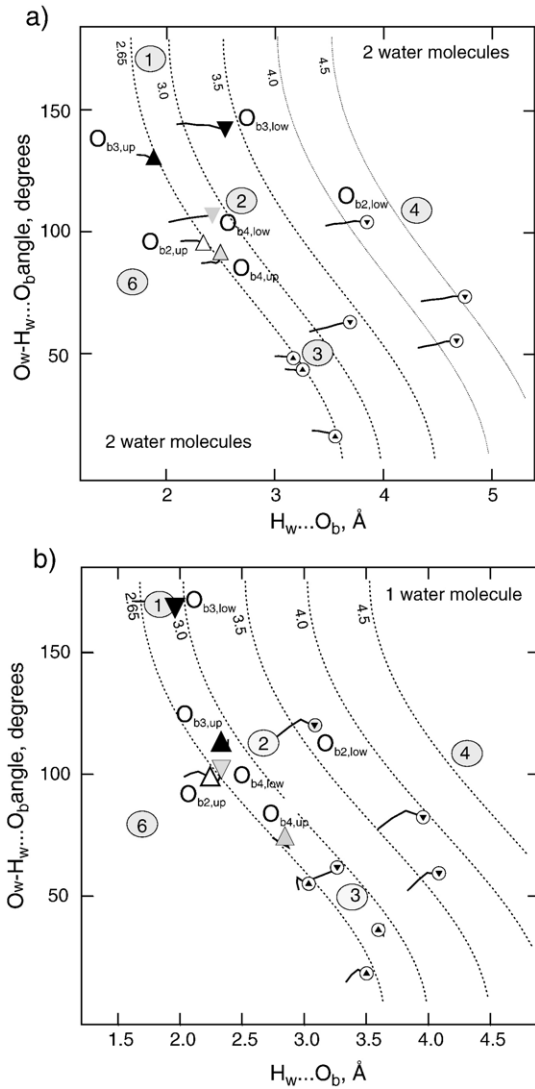


Fig. 10. a) 2 water molecules structure: relations between angles $O_w-H_w...O_b$ vs. $d(H_w...O_b)$. Symbols for $V=220 \text{ \AA}^3$, lines follow smaller volumes results; b) 1 water molecule structure: relations between angles $O_w-H_w...O_b$ vs. $d(H_w...O_b)$. Symbols are for $V=210 \text{ \AA}^3$ and lines follow smaller volumes results. Upward and downward triangles refer to upper basal oxygens (Oup) and lower basal oxygens (Olow) respectively; color and subscript numbers refer to the relative H-bond as indicated in Fig. 6. Dotted lines have been calculated on the basis of the geometrical relation in Steiner and Saenger, 1992 assuming a mean value of $d(H_w-O_w)=0.98$, numbers refer to the related $d(O...O)$ distances. Numbers in the shaded area are, following Steiner and Saenger (1992), 1: two-center and major components of multi-center bonds; 2: minor components of multi-center bonds; 3: non-bonding next neighbors; 4: non-bonding second-next neighbors; 6: chemically forbidden region due to limited $O...O$ approach.

associated with interlayer water behave exactly as those in the $n=0$ structure, and in contrast to those associated with interlayer water according to the values already

quoted. These trends are found in both LDA and GGA, although in detail GGA predicts shorter bonds and smaller angles. In the following, we focus on LDA results, although we note where GGA produce significantly different trends. Interaction of the water molecule with the inner hydroxyl and with basal oxygens is facilitated by rotation of the water molecules (Fig. 8). This rotation is characterized by the angle between the water dipole vector and the $a-b$ plane, θ . In the $n=2$ structure θ increases from 32° at $V=250 \text{ \AA}^3$ to 49° at $V=220 \text{ \AA}^3$ and then changes little upon further compression. In the $n=1$ structure θ increases from 28° at $V=250 \text{ \AA}^3$ to 80° at $V=200 \text{ \AA}^3$ and then decreases slightly on further compression. The orientation of water molecules that we find is consistent with that found in hectorite: Greathouse and Sposito (1998) suggest that water molecules not hydrating the Li^+ counterions are positioned with their dipole moment vector perpendicular to the nearest siloxane surface, i.e. with $\theta=90^\circ$, invoking, as a result, that water is bound to the TOT layers. Semi-empirical molecular dynamics simulations performed by Wang et al. (2004) produce $\theta \approx 30^\circ$ for $n=2$, from 50 to 70° at 5.5 GPa, 750 K for $n=2/3$, and from 0 to 20° at ambient conditions for $n=1$. The internal geometry of the water molecule in the 10 \AA phase is slightly different from that of the free molecule as a result of interactions with the TOT sheets and other water molecules in the condensed phase (Fig. 7b). The most direct comparison is to the geometry of the free molecule computed within the same theoretical framework (Xu and Goddard, 2004). In the 10 \AA phase at the experimental zero pressure volume, the O_w-H_w distance is slightly longer than that in the free molecule, and the $H_w-O_w-H_w$ angle is slightly larger. These differences are consistent with the presence of hydrogen bonded interactions: experimentally, liquid and ice phases of H_2O also show longer O_w-H_w distances and larger $H_w-O_w-H_w$ angles than in the gas phase. In the 10 \AA phase, the O_w-H_w distance and $H_w-O_w-H_w$ angle increase slightly with compression for $n=1$. For $n=2$, the O_w-H_w distance decreases slightly with compression and the $H_w-O_w-H_w$ angle remains approximately constant upon compression.

The strength of hydrogen bonds of the first type (Eq. (1)) is further evaluated according to the $d(O_w...O_i)$ and $\langle O_w...H_i \rangle$ distances and the $O_w...H_i-O_i$ angle (Fig. 9). This hydrogen bond is nearly linear over the entire range studied, with the angle decreasing slightly with compression, but never falling below 172° . The $d(O_w...O_i)$ distance lies in the weak hydrogen bonding regime at the experimental zero pressure volume. On compression, this distance decreases substantially and

falls within the strong hydrogen bonding regime with the stability field of the 10 Å phase. The strong hydrogen bonding regime is characterized by O...O distances 2.5–2.7 Å, and O...H distances 1.5–1.8 Å (Libowitzky, 1999), although it has been suggested that as pressure increases, the regime corresponding to strong hydrogen bonding would shift towards smaller values of the O...O distance (Hofmeister et al., 1999). The $d\langle O_w \dots H_i \rangle$ values in the 10 Å phase also fall within the range of strong hydrogen bonding within the stability field of the 10 Å phase. Hydrogen bonds are stronger in the $n=2$ structure than in the $n=1$ structure. This is due to the water oxygens being pushed closer to the TOT sheets via O_w-O_w and H_w-H_w repulsions.

For the $n=1$ structure, GGA and LDA show large differences in $d\langle O_w \dots O_i \rangle$ and $d\langle O_w \dots H_i \rangle$ at pressures below the stability field of the 10 Å phase, but yield similar results within the stability field. In particular, GGA predicts much larger values of these distances at the experimental zero pressure volume that are in better agreement with the single crystal structure refinement of Comodi et al. (2005). These authors proposed two models that explained the reflections equally well, one in which the water oxygens were located on the mid-plane, and one in which they were located off the mid-plane. The latter model is very similar to our GGA results.

Hydrogen bonds of the second type (Eq. (2)) are bent and asymmetrically multi-furcated. H-bonds involving the upper basal oxygens are generally more bent than those involving the lower basal oxygens. As a result $d\langle H_w \dots O_b \rangle$ rather than $d\langle O_w \dots O_b \rangle$ distances provide better indications of hydrogen bond strength and type. Among all 6+6 possible $O_w-H_w \dots O_b$ bonds, most are weak because of long distances and/or small angles (Fig. 10). The strongest hydrogen bonds within the stability field of the 10 Å phase for the $n=1$ structure are O_3 , low (see Fig. 6 for definition), and for the $n=2$ structure, O_3 , up. These hydrogen bonds fall within the regime of strong hydrogen bonding ($n=2$: $d\langle H_w \dots O_b \rangle = 1.879 \div 1.729$ Å, at $V=220$ Å³ and $V=180$ Å³ respectively; $n=1$ $d\langle H_w \dots O_b \rangle = 1.960 \div 1.605$ Å, at $V=210$ Å³ and $V=180$ Å³ respectively). The $n=2$ structure shows bonds that are more bent ($O_w-H_w \dots O_b$ angles around 131°) as compared with values ranging from 168 to 171° in the $n=1$ structure. Due to the limited distortion of the water molecules with compression in the $n=2$ structure $O_b \dots H_w-O_w$ angles do not significantly change with increasing pressure. The strength of hydrogen bonds with basal oxygens should be evaluated by taking into account that polifurcated H-bond strength is generally underestimated by taking into account only the $d\langle H_w \dots O_b \rangle$ distances, as the main

acceptor capability is enhanced as the number of other acceptors increases (Lutz, 2003).

3. Discussion

3.1. Type of stacking

Our predicted structures largely confirm models proposed on the basis of Raman scattering and X-ray diffraction by Fumagalli et al. (2001). In particular, at ambient pressure we find TOT sheets essentially identical to those in talc with interlayer water bound both to the inner hydroxyl and the basal oxygens. In detail, our first principles results show deviations from the perfect phlogopite-like stacking suggested by Fumagalli et al. (2001).

None of our predicted structures show phlogopite like stacking. This is perhaps not surprising. Unlike the case of phlogopite, the interlayer constituents in our static calculations are non-spherical, so layer offsets might be expected. As our predicted value of the monoclinic angle appears to disagree with the most recent experiments (although there is considerable scatter among previous experimental results at ambient pressure), the key question is how the structure might differ at finite temperature. At finite temperature it is likely that the water molecules rotate, a dynamical mode that we are unable to probe in our static calculations, but which does appear in semi-empirical molecular dynamics calculations. If the water molecules rotate, they would likely behave as more nearly spherical interlayer constituents, perhaps stabilizing phlogopite-like stacking. Moreover, since the energetics governing water rotation are weak at low pressure, water molecules may rotate even at 0 K, due to zero point motion, so that the recent observation that phlogopite-like stacking survives to temperatures as low as 116 K (Zanazzi et al., 2007) may also be explained by water rotation. We note that other modes of stacking have also been found in semi-empirical molecular dynamics simulations, including talc like stacking (Wang et al., 2004).

We expect our static calculations to better represent the experimental situation within the stability field of the 10 Å phase, a range of pressure in which LDA and GGA predictions are in excellent mutual agreement. Because the interlayer collapses rapidly on compression, rotation of water molecules may be suppressed within the stability field and may more closely resemble our static configurations. Indeed, pressure-induced suppression of water rotation has been found in semi-empirical molecular dynamics calculations of the 10 Å phase, in this case described as “freezing” of the interlayer nano-

confined water (Wang et al., 2005). Pressure-induced suppression of anharmonic modes associated with hydrogen bonding has also been suggested in the case of brucite (Mookherjee and Stixrude, 2006).

The experimental situation within the stability field of the 10 Å phase is unclear. Different in situ measurements disagree substantially with each other (Pawley et al., 1995; Comodi et al., 2006), with our theoretical predictions falling between the two experimental results. Comparison is difficult because the experiments were not hydrostatic, because the water content of the experimental samples is not accurately known, and because the structures were refined in different space groups, assuming phlogopite-like stacking (Comodi et al., 2006) or talc-like stacking (Pawley et al., 1995).

3.2. Water bound within the 10 Å phase structure: off the mid-plane or at the center of the interlayer?

We find that water does not occupy the mid-plane of the interlayer except in GGA near ambient pressure and below the stability field of the 10 Å phase. The displacement of the water molecules towards the silicate sheets appears to be crucial for understanding the nature of hydrogen bonding between the interlayer water and the TOT sheets. In particular, bonding to the inner hydroxyl is facilitated by displacement of the water oxygen.

The picture from our theoretical calculations disagrees with that of previous density functional theory calculations and crystal structure refinements at ambient pressure; as yet there is still no experimental data on the location of water molecules at elevated pressure. Bridgeman et al. (1996) using methods similar to ours found that the water molecules lie on the interlayer mid-plane and that the dipole lies in the *a*–*b* plane (Bridgeman et al., 1996). However, this early *ab initio* study was under-converged. In particular, full structural relaxations were not attempted, whereas we fully relax all lattice parameters and atomic positions. Also, computations of Bridgeman et al. (1996) were performed at the Brillouin zone center only, which we found to be insufficient to obtain converged results: we used a $2 \times 2 \times 2$ k-point mesh. Comodi et al. (2005) proposed two models, one in which the water oxygens lie on the mid-plane (Model I), and another in which they are slightly displaced from the mid-plane (Model II). Our GGA results are consistent with the latter model, considering the possible effects of vibrational excitations, which may account for the small remaining difference between our predicted water oxygen positions and those proposed in Model II of Comodi et al. (2005). Our LDA results differ significantly in this

respect, producing water oxygens that lie well off the mid-plane even at zero pressure. Indeed, the position of the water oxygen at low pressure, below the stability field of the 10 Å phase, is one of the largest discrepancies we find between GGA and LDA. However, within the 10 Å phase stability field, GGA and LDA results agree much better with each other and both predict that the water oxygen should lie at least 0.53 Å off the mid-plane within the stability field. Although the interlayer space compresses more rapidly than the distance between water molecules and the TOT sheet, the interactions of water molecules with the TOT structure increase on compression as demonstrated by the decrease in the O_w-H_i and O_w-O_i distances and the increase of the dipole angle with compression. Comodi et al. (2005) propose that interlayer water forms hydrogen bonds only with the basal oxygens, and not with the inner hydroxyl. They envision the water dipole pointing away from the nearest TOT sheet, rather than towards the TOT sheet as in our results, so that only the water hydrogens interact with the TOT sheet. It is important to remember in this context that the experiments of Comodi et al. (2005) are not capable of locating hydrogens. The location of water molecules off the mid-plane and tilted towards the TOT sheets, as we envision the structure, is in agreement with molecular dynamics simulations based on semi-empirical potentials (Wang et al., 2004).

Raman spectra of the 10 Å phase also argue for hydrogen bonding between the inner hydroxyl and interlayer water. The hydroxyl stretching frequency in the 10 Å phase (3622 cm^{-1}) is substantially smaller than that in talc (3677 cm^{-1}) (Fumagalli et al., 2001). These results are consistent with the absence of hydrogen bonding in talc and the presence of hydrogen bonding in the 10 Å phase. High pressure Raman spectroscopy of the 10 Å phase shows that the inner hydroxyl stretching frequency increases with pressure (Comodi et al., 2006), whereas hydrogen bonds typically show a decrease with compression. However, the inner hydroxyl in the 10 Å phase and talc may not be typical. The inner hydroxyl interacts strongly not only with the water oxygen, but also with surrounding cations. For example, at the experimental zero pressure volume, the distance between H_i and the surrounding Mg cations is only 2.7 Å. Indeed, previous studies have found that the inner hydroxyl stretching frequency is significantly influenced by the cations occupying the octahedral sites (Velde, 1983). Such interactions may be responsible for the increase with pressure of the inner hydroxyl stretching frequency as observed in talc (Holtz et al., 1993; Scott et al., submitted for publication) and may

also be responsible for some part of the pressure-induced increase seen in the 10 Å phase. The 10 Å phase results may also be significantly influenced by the presence of non-hydrostatic stress in the experiments of Comodi et al. (2006). Further experimental studies should investigate the behavior of the 10 Å phase in a quasi-hydrostatic environment.

3.3. Compressibility behavior and water content

We find that the volume and bulk modulus of the 10 Å phase depends significantly on water content, a relationship that may be useful in constraining the water content of experimental samples. We find that the theoretically predicted $n=2$ volume at ambient conditions and after correcting for phonon excitation is very similar to experiment. The water-bearing structures are stiffer than talc due to 1) the stronger interlayer bonding (K_c) and 2) water–water repulsion, and “stuffing” of the hexagonal rings of the T sheet (K_a , K_b); the $n=2$ structure is somewhat softened as compared with the $n=1$ structure because the additional water expands the structure substantially, thereby partially counteracting effects 1 and 2. Quantitative comparison with existing experimental data is made difficult by the significant differences between experiments. The origin of the discrepancy between experimental and theoretical values of K_0 is unclear in part because of experimental uncertainties associated with non-hydrostatic stress and the non-uniqueness of equation of state fitting, as discussed above. An independent determination of the bulk modulus of the 10 Å phase via Brillouin spectroscopy would be valuable.

All three structures investigated are energetically stable under static conditions, favouring the idea of a variable amount of water that can be incorporated into the 10 Å phase. Raman spectra (Fumagalli et al., 2001) also support the $n=2$ structure: three peaks in the OH stretching region, a condition satisfied by the $n=2$ structure for which the structural environment of each water molecules, and each hydroxyl, is identical. In contrast, the $n=1$ structure would be expected to produce at least one additional peak since in this structure, there are two distinct hydroxyl environments: half bound to water molecules, and half not. Welch et al. (2006) recently suggested the presence of a hydrogarnet substitution ($\text{Si} \rightarrow 4\text{H}$) within the 10 Å phase structure based on microprobe analysis and NMR spectroscopy performed on synthetic samples. Our calculations, together with previous Raman spectroscopy (Fumagalli et al., 2001) do not support the structure proposed by Welch et al. (2006). In particular, the presence of $(\text{OH})_4$

groups in the T sheet would produce additional unobserved OH-stretching frequencies, and alter the selection rules so as to produce additional unobserved peaks in the Si–O stretching, Si–O bending, and Mg–O stretching and bending regions (Kolesov and Geiger, 2005). All observed Raman modes are accounted for by assuming that the 10 Å phase consists of TOT sheets identical to those in talc, with interlayer water interacting with both the inner hydroxyl and the basal oxygens.

4. Implications

Interaction of the 10 Å phase with other micas is suggested by its phlogopite-like stacking, which we attribute to rotational excitations of the water molecules. Indeed mixed layer silicates exist between not perfectly isostructural phases, such as chlorite and talc that form the mineral kulkeite found in nature (Schreyer et al., 1982). That the 10 Å phase might interact with phlogopite has been suggested on the basis of high pressure experiments in K-bearing ultramafics (Fumagalli, 2003; Zanchetta et al., 2005). Mineral chemistry of high pressure phlogopites show a generalized, pressure dependent K deficiency along the exchange vector $\text{K}_{-1}\text{Al}_{-1}\text{Si}_{1\dots 1}$, that drives the phyllosilicate composition toward a “talc component”. Due to the chemical analogy of the 10 Å phase with talc and its stability at higher pressure as compared with the stability of talc in ultramafics, a chemical shift towards the 10 Å phase, might also be envisaged. The relevance of a “talc/10 Å phase” component in synthesised phlogopites has been also indicated in other bulk compositions: Hermann (2002) investigating felsic rocks at pressures in the ranges 2.0–4.0 GPa and 780–900 °C, found that phlogopite, with increasing pressure, preferentially follows the $\text{K}_{-1}\text{Al}_{-1}\text{Si}_{1\dots 1}$ exchange vector rather than forming solid solutions with phengite; Wunder and Melzer (2003) found up to 29 mol% of interlayer vacancies in three series of synthetic phlogopites (Rb-series, Cs-series and Ba-series) at 0.2–2.0 GPa and 700–800 °C.

Whether the interactions between phlogopite, chlorite and the 10 Å phase involve order–disorder relations or crystal chemical substitution cannot be envisaged on the basis of data so far available. Nonetheless, evidence of Al (and K) solubility within the structure of the 10 Å phase has been found: Bauer and Sclar (1981) pointed out the lack of incorporation of K and Al within the 10 Å phase structure in high pressure synthesis run products; on the other hand the Al-bearing 10 Å phase observed in ultramafic compositions (Fumagalli and Poli, 2005) is better described as related to mixed layered silicates

rather than to simple tschermak substitution. The fact that a mixed layer model is preferred rather than cation solubility in mica-like structures, suggests that, in order to observe interactions between phlogopite, chlorite and the 10 Å phase, a true isostructural character is not required. Furthermore, the ability of the 10 Å phase to interact with other phyllosilicates (micas and chlorite) and the fact that these interactions are not restricted to mica-like structures, makes this phase of relevance in a wider range of compositions and P and T conditions at which mica structures are not stable.

Furthermore the fact that water molecules are stably bound within the 10 Å structure is of relevance since it would be the first case among the DHMS group minerals, although it would not be the only example of bound water in a phyllosilicate (e.g. hectorite, Greathouse and Sposito, 1998). It opens therefore a new scenario in the evaluation of the water cycle within the Earth mantle.

Acknowledgements

This work was supported by MIUR-COFIN 2005 (PF) and by the National Science Foundation under grant EAR-0230154 (LS).

References

- Anderson, O.L., Nafe, J.E., 1965. Bulk modulus-volume relationship for oxide compounds and related geophysical problems. *J. Geophys. Res.* 3951–3960.
- Angel, R.J., Frost, D.J., Ross, N.L., Hemley, R., 2001. Stabilities and equations of state of dense hydrous magnesium silicates. *Phys. Earth Planet. Inter.* 127, 181–196.
- Bailey, S.W., 1998. Introduction. In: Bailey, S.W. (Ed.), *Rev. Mineral.*, vol. 19. Mineral. Soc. Am., Washington, DC, pp. 1–8.
- Bauer, J.F., Sclar, C.B., 1981. The “10 Å phase” in the system MgO-SiO₂-H₂O. *Am. Mineral.* 66, 576–585.
- Bridgeman, C.H., Skipper, N.T., 1997. A Monte Carlo study of water at an uncharged clay surface. *J. Phys., Condens. Matter* 9, 4081–4087.
- Bridgeman, C.H., Buckingham, A.D., Skipper, N.T., Payne, M.C., 1996. Ab-initio total energy study of uncharged 2:1 clays and their interaction with water. *Mol. Phys.* 89, 879–888.
- Chinnery, N.J., Pawley, A.R., Clark, S.M., 1999. In situ observation of the formation of 10 Å phase from talc + H₂O at mantle pressures and temperatures. *Science* 286, 940–942.
- Comodi, P., Fumagalli, P., Montagnoli, M., Zanazzi, P.F., 2004. A single crystal study on the pressure behavior of phlogopite and petrological implications. *Am. Mineral.* 89, 647–653.
- Comodi, P., Fumagalli, P., Nazzareni, S., Zanazzi, P.F., 2005. The 10 Å phase: crystal structure from X-ray single-crystal data. *Am. Mineral.* 90, 1012–1016.
- Comodi, P., Cera, F., Dubrovinsky, L., Nazzareni, S., 2006. The high pressure behaviour of the 10 Å phase: a spectroscopic and diffractometric study up to 42 GPa. *Earth Planet. Sci. Lett.* 246, 444–457.
- Cygan, R.T., Liang, J., Kalinichev, A.G., 2004. Molecular models of hydroxide, oxyhydroxide, and clay phases and the development of a general force field. *J. Phys. Chem., B* 108, 1255–1266.
- Duffy, T.S., Russell, J.H., Mao, H., 1995. Equation of State and shear strength at multimegabar pressures: magnesium oxide to 227 GPa. *Phys. Rev. Lett.* 74, 1371–1374.
- Frost, D.J., 1999. The stability of dense hydrous magnesium silicates in Earth’s transition zone and lower mantle. In: Fei, Y.-W., Bertka, C., Mysen, B.O. (Eds.), *Mantle Petrology: Field Observations and High Pressure Experimentation: a Tribute to Francis R. (Joe) Boyd*. The Geochemical Society, Special Publication, vol. 6, pp. 283–296.
- Fu, M.H., Zhang, Z.Z., Low, P.F., 1990. Changes in the properties of a montmorillonite-water system during the adsorption and desorption of water: hysteresis. *Clays Clay Miner.* 5, 485–492.
- Fumagalli, P., 2003. Subsolidus phase relations in K-doped lherzolites and the composition of phlogopite to 6.0 GPa: an experimental study. *Geophysical Research Abstracts*, vol. 5, p. 12436.
- Fumagalli, P., Poli, S., 2005. Experimentally determined phase relations in hydrous peridotites to 6.5 GPa and their consequences on the dynamics of subduction zones. *J. Petrol.* 46, 555–578.
- Fumagalli, P., Stixrude, L., Poli, S., Snyder, D., 2001. The 10 Å phase: a high-pressure expandable sheet silicate stable during subduction of hydrated lithosphere. *Earth Planet. Sci. Lett.* 186, 125–141.
- Greathouse, J., Sposito, G., 1998. Monte Carlo and molecular dynamics studies of interlayer structure in Li(H₂O)₃-smectites. *J. Phys. Chem., B* 102, 2406–2414.
- Hermann, J., 2002. Experimental constraints on phase relations in subducted continental crust. *Contrib. Mineral. Petrol.* 143, 219–235.
- Hofmeister, A.M., Cynn, H., Burnley, P.C., Meade, C., 1999. Vibrational spectra of dense, hydrous magnesium silicates at high pressure: importance of hydrogen bond angle. *Am. Mineral.* 84, 454–464.
- Holtz, M., Solin, S.A., Pinnavaia, T.J., 1993. Effect of pressure on the Raman vibrational-modes of layered aluminosilicate compounds. *Phys. Rev., B* 13312–13317.
- Kishina, N.R., Wirth, R., Andrut, M., Ukhanov, A.V., 2001. Extrinsic and intrinsic mode of hydrogen occurrence in natural olivines: FTIR and TEM investigation. *Phys. Chem. Miner.* 28, 291–301.
- Kresse, G., Furthmüller, J., 1996a. Efficiency of ab-initio total energy calculations for metals and semiconductors. *Comput. Mater. Sci.* 6, 15–50.
- Kresse, G., Furthmüller, J., 1996b. Efficient iterative schemes for ab initio total-energy calculations using a plane-wave basis set. *Phys. Rev., B* 54, 11169–11186.
- Kresse, G., Hafner, J., 1993. Ab initio molecular-dynamics for liquid-metals. *Phys. Rev., B* 47, 558–561.
- Kresse, G., Hafner, J., 1994. Norm-conserving and ultrasoft pseudopotential for first-row and transition-elements. *J. Phys., Condens. Matter* 8245–8257.
- Kolesov, B.A., Geiger, C.A., 2005. The vibrational spectrum of synthetic hydrogrossular (katoite) Ca₃Al₂(O₄H₄)₂: a low temperature IR and Raman spectroscopic study. *Am. Mineral.* 90, 1335–1341.
- Libowitzky, E., 1999. Correlation of O–H stretching frequencies and O–H...O hydrogen bond lengths in minerals. *Monatsh. Chem.* 130, 1047–1059.
- Libowitzky, E., Rossman, G.R., 1996. FTIR spectroscopy of lawsonite. *Am. Mineral.* 81, 1080–1091.
- Lutz, H.D., 2003. Structure and strength of hydrogen bonds in inorganic solids. *J. Mol. Struct.* 646, 227–236.
- Monkhorst, H.J., Pack, J.D., 1976. Special points for brillouin-zone integrations. *Phys. Rev., B* 13, 5188–5192.

- Mookherjee, M., Stixrude, L., 2006. High-pressure proton disorder in brucite. *Am. Mineral.* 91, 127–134.
- Pavese, A., Levy, D., Curetti, N., Diella, V., Fumagalli, P., Sani, A., 2003. Equation of state and compressibility of phlogopite by in situ X-ray powder diffraction. *Eur. J. Mineral.* 15, 455–463.
- Pawley, A.R., Redfern, S.A.T., Wood, B.J., 1995. Thermal expansivities and compressibilities of hydrous phases in the system MgO–SiO₂–H₂O: talc, phase A and 10-Å phase. *Contrib. Mineral. Petrol.* 122, 301–307.
- Pawley, A.R., Welch, M.D., Smith, R.I., 2004. The 10-Å phase: structural constraints from neutron powder diffraction. *Lithos* 73, 1–2 (S86).
- Perdikatsis, B., Burzlaff, H., 1981. Structural refinement of talc Mg₃[(OH)₂Si₄O₁₀]. *Z. Kristallogr.* 156, 177–186.
- Robinson, K., Gibbs, G.V., Ribbe, P.H., 1971. Quadratic elongation — quantitative measure of distortion of coordination polyhedra. *Science* 172, 567–569.
- Schreyer, W., Medenbach, O., Abraham, K., Gebert, W., Müller, W.F., 1982. Kulkeite a new metamorphic phyllosilicate mineral: ordered 1:1 chlorite/talc mixed-layer. *Contrib. Mineral. Petrol.* 80, 103–109.
- Sclar, C.B., Carrison, L.C., Schwartz, C.M., 1965. High-pressure synthesis and stability of a new hydronium-bearing layer silicate in the system MgO–SiO₂–H₂O. *Trans. - Am. Geophys. Union* 46, 184.
- Scott, H.P., Liu, Z., Hemley, R.J., Williams, Q., submitted for publication. High-pressure infrared spectra of talc and lawsonite. *Am. Mineral.*
- Sposito, G., Prost, R., 1982. Structure of water adsorbed on smectites. *Chem. Rev.* 6, 553–573.
- Steiner, T.H., Saenger, W., 1992. Geometric analysis of non-ionic O–H... O hydrogen bonds and non-bonding arrangements in neutron diffraction studies of carbohydrates. *Acta Crystallogr.* B 48, 819–827.
- Stixrude, L., 2002. Talc under tension and compression: spinodal instability, elasticity, and structure. *J. Geophys. Res.* 107 (B12), 23–27.
- Vanderbilt, D., 1990. Soft self-consistent pseudopotentials in a generalized eigenvalue formalism. *Phys. Rev.*, B 41, 7892–7895.
- Velde, B., 1983. Infrared OH-stretch bands in potassic micas, talcs and saponites — influence of electronic configuration and site of charge compensation. *Am. Mineral.* 1169–1173.
- Viani, A., Gaultieri, A.F., Artioli, G., 2002. The nature of disorder in montmorillonite by simulation of X-ray powder patterns. *Am. Mineral.* 87, 966–975.
- Wang, J., Kanilichev, A.G., Kirkpatrick, R.J., 2004. Molecular modelling of the 10-Å phase at subduction zone conditions. *Earth Planet. Sci. Lett.* 222, 517–527.
- Wang, J., Kanilichev, A.G., Kirkpatrick, R.J., 2005. Structure and decompression melting of a novel, high-pressure nanoconfined 2-D ice. *J. Phys. Chem.*, B 109, 14308–14313.
- Welch, M.D., Pawley, A.R., Ashbrook, S.E., Mason, H.E., Phillips, B.L., 2006. Si vacancies in the 10-Å phase. *Am. Mineral.* 91, 1707–1710.
- Wunder, B., Melzer, 2003. Interlayer vacancy characterization of synthetic phlogopitic micas by IR spectroscopy. *Eur. J. Mineral.* 14, 1129–1138.
- Wunder, B., Schreyer, W., 1992. Metastability of the 10 Å phase in the system MgO–SiO₂–H₂O (MSH). What about hydrous MSH phases in subduction zones? *J. Petrol.* 33, 877–889.
- Xu, X., Goddard, W.A., 2004. Bonding properties of the water dimer: a comparative study of density functional theories. *J. Phys. Chem.*, A 108 (12), 2305–2313.
- Zanazzi, P.F., Comodi, P., Nazzareni, S., Rotiroli, N., van Smaalen, S., 2007. Behavior of 10-Å phase at low temperature. *Phys. Chem. Miner.* 34, 23–29.
- Zanchetta, S., Fumagalli, P., Poli, S., 2005. Phase relations in amphibole-bearing ultramafics: experimental results up to 3 GPa and 1000 °C. *Epitome* 1, 143.